

Biaxial properties of individual bonds in thermomechanically bonded nonwoven fabrics

Textile Research Journal
89(5) 698–710
© The Author(s) 2018
Article reuse guidelines:
sagepub.com/journals-permissions
DOI: 10.1177/0040517517753640
journals.sagepub.com/home/trj


RS Wijeratne¹, R De Vita¹, JA Rittenhouse^{1,2}, EB Orlor²,
RB Moore² and DA Dillard¹

Abstract

Thermomechanically bonded nonwoven fabrics contain discrete bonds that are formed from melted and fused fibers. In these fabrics, the fibers are loosely organized although they lie predominantly in the machine direction (MD). Through a custom-built biaxial testing device and simultaneous image capture, the mechanical response of individual bonds in thermomechanically bonded nonwoven fabrics made of polyethylene/polypropylene sheath–core fibers was studied. Toward this end, cruciform specimens ($n=20$) with bonds in the gauge areas and arms aligned in the MD and the cross-direction (CD) were subjected to displacement-controlled equi-biaxial tests. The biaxial force–displacement curves along the two loading directions were found to be different. The average maximum force and average stiffness were significantly higher in the MD than in the CD ($p < 0.05$). This difference was determined by the amount and orientation of fibers and size of the bonds in the two directions. By analyzing the images captured during equi-biaxial testing, the bonds were always observed to disintegrate into their constituent fibers. Digital image correlation was used to measure the local and average Eulerian strains of the bonds before their breakage initiated. The average axial strain experienced by the bond in the MD was always monotonically increasing with the axial load. The average axial strain in the CD, however, varied among bonds: it was monotonically increasing, monotonically decreasing, and increasing and decreasing with the axial load. Strain maps demonstrated the inhomogeneity in strain experienced by the bonds. These findings can guide the design and development of thermomechanically bonded nonwoven fabrics for applications in automotive, medical, consumer products, and civil engineering industries.

Keywords

biaxial tests, thermomechanically bonded nonwoven, mechanical properties, digital image correlation, material behavior

Nonwoven fabrics are utilized by numerous industries, including, but not limited to, the automotive, medical, consumer products, and civil engineering industries. Nonwoven fabrics are designed and engineered to provide the required functionality, while being a cheaper alternative to woven fabrics.¹ There are different manufacturing processes used to form nonwovens, such as staple fiber carding, melt-blowing, and spunbonding processes. In spunbond technology, the nonwoven fabrics are made from raw polymer pellets that are extruded to form fibers. These fibers are laid onto a conveyor belt in an unorganized fashion, undergo bonding, and, occasionally, an additional post-processing treatment. The spunbond nonwoven process is schematically depicted in Figure 1.

In a nonwoven fabric, the fibers are the most important mechanical elements. Fiber characteristics, including polymer type, composition, and size, have been shown to impact the strength of fabrics.² The fibers are homo-component for some end use applications but, in recent years, bi-component fibers have been

¹Department of Biomedical Engineering and Mechanics, Virginia Tech, Blacksburg, VA, USA

²Department of Chemistry, Virginia Tech, Blacksburg, VA, USA

Corresponding author:

R De Vita, Virginia Polytechnic Institute and State University, 335 Kelly Hall, Blacksburg, VA 24061-0131, USA.
Email: devita@vt.edu

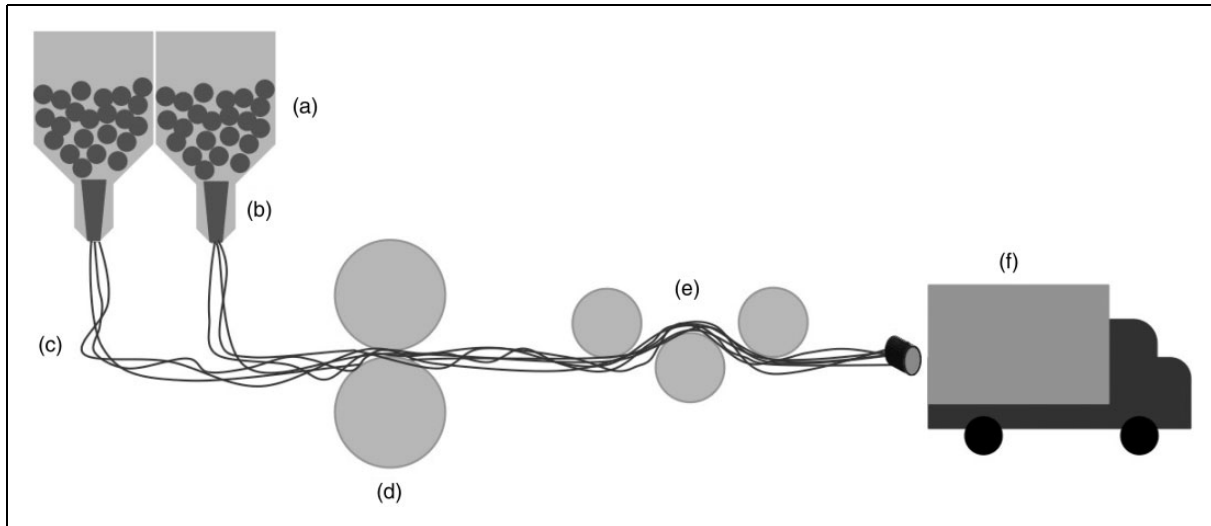


Figure 1. Spunbond nonwoven manufacturing process: (a) the raw pellets are (b) melted and (c) formed into fibers. The fibers undergo (d) a bonding process and (e) an optional post-processing prior to being (f) shipped to customers.

employed to tailor the properties of the fabrics for use in a large range of applications. Typically, two polymers, such as polyethylene (PE) and polypropylene (PP), are used to create fibers with various cross-sectional geometries (e.g., sheath–core, side by side, and islands-in-the-sea).^{3–5}

Together with the fibers, the bonds are crucial in determining the mechanical properties of nonwovens. Several studies have shown that the bonds dictate the stiffness and strength of nonwovens.² Mechanical, chemical, and thermal bonding techniques are used to create bonds and these techniques are often combined. For example, in thermomechanically bonded nonwovens, thermal and mechanical bonding techniques are combined to increase the production rates,⁶ as schematically illustrated in Figure 2. Briefly, a fibrous mat is passed through a heated calender roll. The heat softens the fibers and then nips on the calender roll (of variable size, shape, and design symmetry) weld the fibers together when opposing rolls come in close contact, thus forming discrete bonds. In thermomechanically bonded nonwovens with sheath–core fibers, the polymer of the sheath often has a lower melting point and serves an adhesive while the polymer of the core has a higher melting point so that the fiber can maintain the original integrity. Due to the movement of the fibers along the belt and through the calender roll, the nonwoven has a preferential fiber direction that is parallel to the direction of the belt. This preferential fiber direction is referred to as the machine direction (MD), while the direction that is perpendicular to the MD in the plane of the nonwoven is the cross-direction (CD).

The organization of the fibers and the discrete bonds lead to highly anisotropic thermomechanically bonded

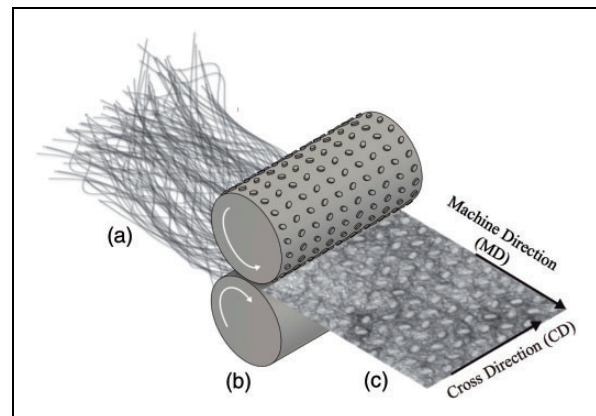


Figure 2. Schematics of the thermomechanical bonding process where (a) a web of fibrous material is passed through (b) a heated calender roll with nips. These nips melt and weld fibers together, forming (c) discrete bonds. Machine direction (MD) and cross-direction (CD) are also shown.

nonwoven fabrics,⁷ which demonstrate unique deformation behavior. In order to gain insight into the deformation mechanisms, uniaxial tensile tests are commonly performed on coupons of nonwovens with dimensions of the order of centimeters.^{8–12} The deformation of individual bonds within the specimens has been observed, but never quantified. Nanjundappa and Bhat¹³ studied individual bonds within a nonwoven specimen, analyzing the effect of bonding temperature on the failure mechanism of individual bonds. Similarly, Kim et al.,¹⁴ while testing nonwoven specimens bonded at various temperatures, investigated the failure mechanism of individual bonds. The most

complete quantitative characterization of individual bonds was performed by Bhat et al.¹⁵ These authors examined how the bond (e.g., bonding temperature, bond size, and area) affected the uniaxial peak load and tear strength of nonwovens by testing small strip specimens (80 mm × 5 mm) in the MD and CD.

Biaxial tensile tests have been performed on nonwoven fabrics, but at a larger scale than individual bonds. Goswami et al.¹⁶ used biaxial tests of nonwovens in order to determine the Poisson's ratios in thermally bonded nonwoven fabrics. It was determined that biaxial tests, rather than uniaxial tests, provided a more accurate estimate of the Poisson's ratios of nonwovens. The base fibers of the nonwovens dominated the biaxial response, while the uniaxial response was mainly determined by the binder film between fibers.

Recently, the digital image correlation (DIC) method has been used to measure strain in nonwovens and validate finite element models.^{17–19} In order to use this method, a random speckle pattern is created on the surface of the specimen to be tested. While performing the desired mechanical test (i.e., uniaxial tensile test), images of this surface are recorded. The movement of the speckle pattern is then reconstructed via computer software and the strain map of the specimen is computed. The DIC method enables the measurement of large, nonlinear, and inhomogeneous strain,²⁰ which are typical of nonwovens. While studying the effects of testing temperature and strain rate on PP nonwoven fabrics, Jubera et al.¹⁸ utilized the DIC method in order to measure the strains at a macroscopic level. Additional work was recently performed by Ridruejo et al.¹⁹ to measure strains through the DIC method in notched nonwoven specimens subjected to uniaxial tensile tests. The authors found that the strength of the notched specimen was higher than the strength of the unnotched counterpart due to the microstructure of the nonwoven.

This study focuses on understanding the mechanical behavior of thermomechanical bonds in nonwoven fabrics. Toward this end, cruciform nonwoven specimens with individual bonds in their central regions and with arms aligned along the MD and CD are biaxially tested. The difference between the responses along the MD and CD is analyzed and interpreted by considering the fiber organization and the bond geometry. Images of the bonds during biaxial testing are also collected in order to perform strain measurements using the DIC method. By using biaxial force–displacement data and the strain data, the material anisotropy and strain inhomogeneity of the bonds not only can be visualized, but can also be quantified. The outcome of this study will be crucial to systematically control the integrity of the bonds during the thermomechanical bond process and determine suitable applications of the produced nonwovens.

Materials and methods

Specimen preparation

Commercial bi-component thermomechanically spun-bonded nonwoven fabric was obtained to test the biaxial properties of individual bonds within the fabric. The fabric was composed of PE/PP sheath–core fibers and had an average basis weight of 20 gsm (grams per square meter). Prior to mechanical testing, the nonwoven fabric sheet was scanned using an optical transmission scanner (Epson Perfection V850 Pro) at 16-bit grayscale and 2540 dpi (dots per inch). Relative basis weight of square regions measuring 2 mm × 2 mm, centered around individual bonds and with sides aligned along the MD and CD, were analyzed using ImageJ software (ImageJ, National Institute of Health, MD, USA).²¹ More specifically, the relative basis weight, B_{rel} , was measured using the Beer–Lambert law

$$B_{rel} = \ln\left(\frac{I_0}{I}\right) \quad (1)$$

where I and I_0 are the intensities of the incident light measured using the optical transmission scanner in areas with and without the nonwoven fabric, respectively.

The relative basis weight assumed values between 0 and 1, where zero signified no light absorption (i.e., no material present) and unity represented complete light absorption. Once such quantity was computed on over 300 randomly chosen square regions, centered around the bonds and with sides oriented along the MD and CD, 20 of these regions with comparable relative basis weight (0.348 ± 0.002 , mean \pm S.D.) were selected. This selection helped reduce variation among the tested specimens.

In order to clamp the bonds, nonwoven cruciform specimens with arms oriented along the MD and CD and width of 3 mm were cut using micro-scissors so that their centers contained the square regions with the bonds to be tested. Polyethylene terephthalate glycol (PTEG) sheets having a 0.25 mm thickness (Thick Clear Plastic Sheet, K&S Precision Metals) were also cut using a laser cutter (VLS3.60, Universal Laser System) to create mounting frames for the nonwoven cruciform specimens. Details about the mounting frame and its dimensions are illustrated in Figure 3. As shown in Figure 3, the center of the mounting frames featured a 2 mm × 2 mm square window within which the bond to be tested had to be centered.

The cruciform nonwoven specimen was then attached to the mounting frame using double-sided tape (Scotch Double Sided Permanent Tape, 3M) to place the bond in the center of the mounting frame, precisely in the square window. Four notches were

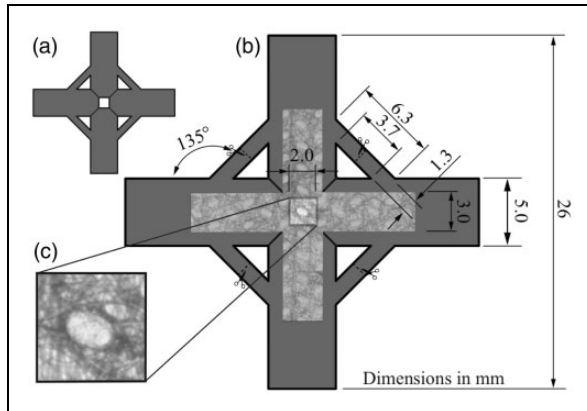


Figure 3. Schematics of the nonwoven specimen over a plastic frame: (a) plastic frame with a 2 mm \times 2 mm square window; (b) nonwoven cruciform specimen on plastic frame; (c) bond in the center of the 2 mm \times 2 mm square window of the plastic frame.

created on the cruciform specimen outside the 2 mm \times 2 mm square region along the diagonal directions using micro-scissors. This was done to reduce the gauge length of the square region containing the bond from 3 to 2 mm. Using a quick curing epoxy recommended for bonding polyolefins (J-B Weld 50133 Plastic Bonder), the cruciform specimen region outside the 2 mm \times 2 mm square window was completely secured on the mounting frame.

A random speckle pattern was created on each specimen using an airbrush (Badger 150, Badger Air Brush Co.) with a fine needle (Badger Fine Needle for #100 and #150, Badger Air Brush Co.) and India ink (Super Black India ink, Speedball). The fine random speckle pattern was needed for the non-contact strain measurements performed upon the completion of the biaxial test.

Biaxial tensile testing

A biaxial tensile testing machine was custom-built for testing the single bonds selected from the nonwoven fabric. Four linear actuators (Linear actuator, 25 mm travel, RS-232 plus manual control, Zaber Technologies Inc.) were used to control the motion along two perpendicular axes. Two 8.9 N (2lb.) load cells (Jr. Miniature S-Beam Load Cell, FUTEK Advanced Sensor Technology, Inc.) were mounted to two adjacent actuators. Custom-built mechanical clamps with embedded nuts were designed and made using a three-dimensional (3D) printer (Replicator, MakerBot). The clamps were then attached to either the actuators or the load cells. In order to collect images of the specimen during biaxial testing, an Extended Graphics Array (XGA) camera (Stingray

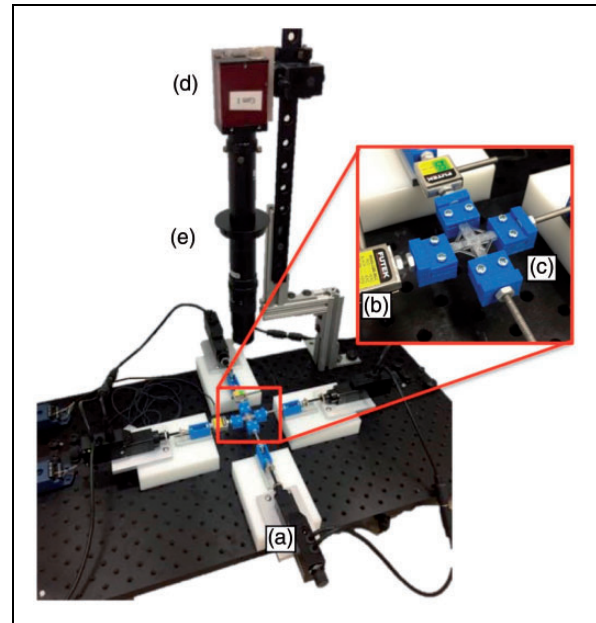


Figure 4. Custom-built biaxial tensile test stage with (a) four linear actuators, (b) two load cells, (c) four three-dimensional printed clamps (shown with specimen loaded for testing), (d) camera, and (e) lens.

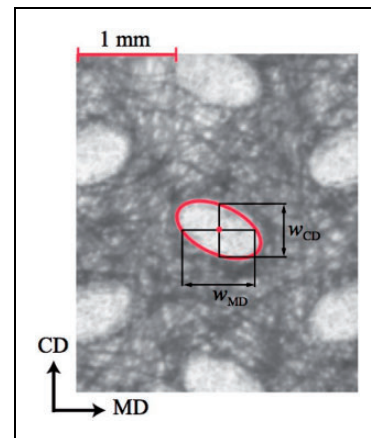


Figure 5. Definition of bond width, w , in the machine direction (MD) and cross-direction (CD).

F-080, Allied Vision Technologies) equipped with a 0.7X-4.5X lens (VZM 450i Zoom Imaging Lens, Edmund Optics) was used. The complete biaxial tensile test stage, with a specimen loaded for testing, can be seen in Figure 4. A LabVIEW program (LabVIEW, National Instruments) was developed to control the actuators as well as record images of the bond, actuator displacements, and loads during biaxial testing.

Equi-biaxial tests were performed at room temperature (approximately 20°C) at a constant 0.1 mm/s displacement rate (resulting in a nominal strain rate within

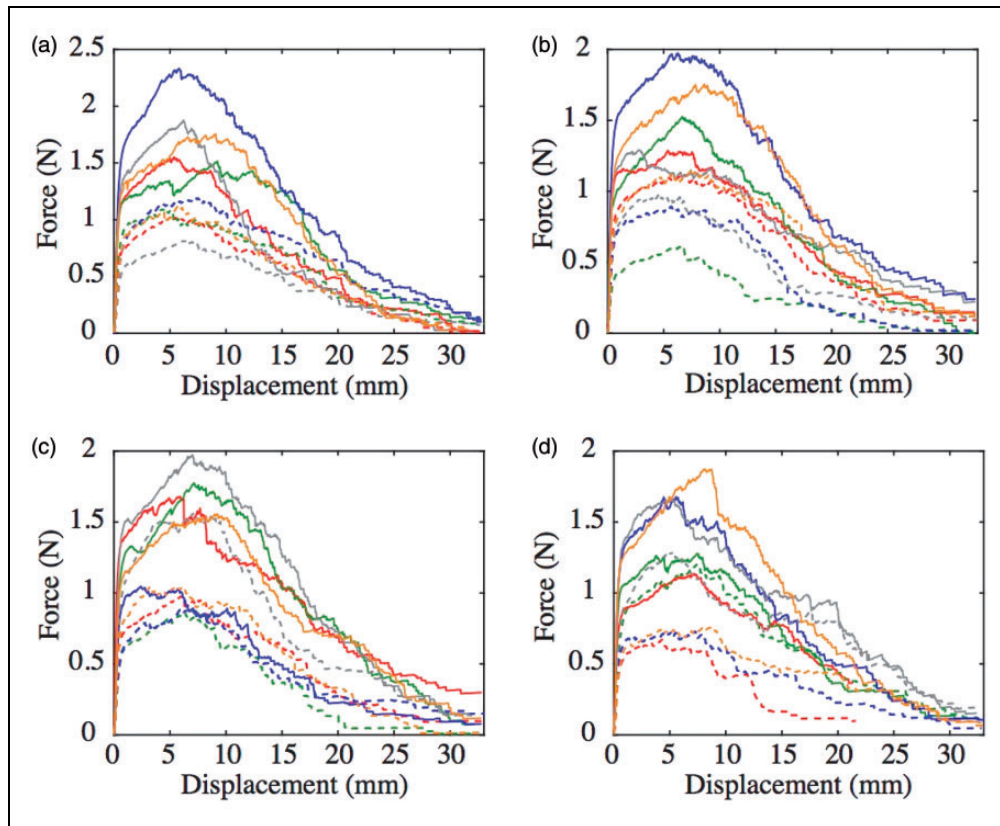


Figure 6. Force–displacement data for (a) specimens 1–5, (b) specimens 6–10, (c) specimens 11–15, and (d) specimens 16–20. The solid line denotes the machine direction force–displacement data, while the dotted line in the identical color represents the corresponding cross-direction force–displacement data. (Color online only.)

the tested region of 5%/s) on $n=20$ specimens. Once each nonwoven cruciform specimen on the mounting frame was attached to the clamps, the diagonal braces of the mounting frame were cut to allow movement of the $2\text{ mm} \times 2\text{ mm}$ central square region of the specimen along the two loading axes (locations of the cuts in the mounting frame are shown as the scissor marks in Figure 3). The specimen was preloaded to 0.01 N in both loading directions and was then equi-biaxially stretched until either failure in both directions occurred or one of the actuator's physical travel limits was reached.

Strain analysis

Image sequences of each speckled bond within the $2\text{ mm} \times 2\text{ mm}$ central square region of the cruciform specimen were used to calculate the evolving in-plane strain maps using an open source DIC software package written in MATLAB (MATLAB 2016, Mathworks).²² The software was modified to manually select four speckles and track their motion to calculate the in-plane Eulerian–Almansi strain components, e_{xx} , e_{yy} , and e_{xy} where the x -axis and the y -axis

coincide with the MD and CD, respectively. Due to bond disintegration during testing, strain analysis was performed up to 2.3 mm axial displacement along the MD and CD.

Orientation analysis

Scanned images ($n=20$) of the $2\text{ mm} \times 2\text{ mm}$ regions centered on bonds and selected for testing were also analyzed using the OrientationJ plugin²³ in ImageJ to determine fiber orientation.^{21,24} The output of the OrientationJ plugin was a count of pixels oriented at each angle from -90° to 89° , in 1° increments. This provides a function $f(\theta)$ that defines the frequency of fibers at each angle θ . From the orientation distribution, orientation parameters were calculated for each specimen. Based on Cox's analysis of the strength of paper and other fibrous materials,²⁵ the orientation parameter, O_p , was assumed to have the following form

$$O_p = \frac{\int_{-\pi/2}^{\pi/2} f(\theta) \cos^4 \theta d\theta}{\int_{-\pi/2}^{\pi/2} f(\theta) d\theta} \quad (2)$$

where θ is the orientation angle and $f(\theta)$ is the frequency at each orientation angle. The orientation parameter is a dimensionless quantity with a value between 0 and 1, where unity indicated that all the fibers are perfectly

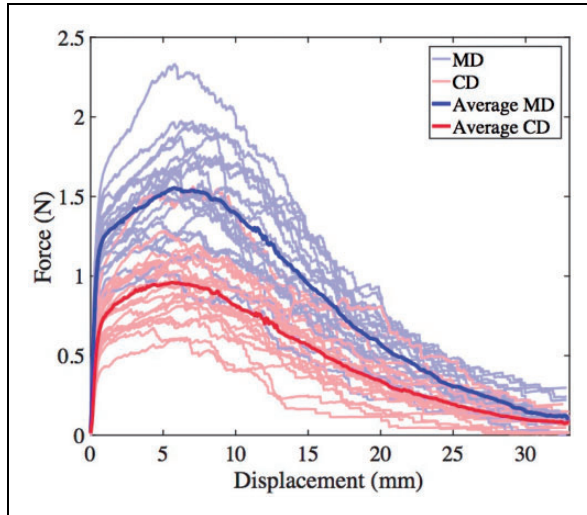


Figure 7. Average force–displacement curves and force–displacement curves from the tested specimens ($n = 20$). MD: machine direction; CD: cross-direction.

aligned at 0° and zero indicates that all the fibers are perfectly aligned perpendicular to 0° . In this analysis, 0° was selected to be the MD when computing O_p in the MD and was assumed to be the CD when computing O_p in the CD.

Force–displacement data analysis

The stiffness of the bond in the MD or CD was defined as the slope of the line that fitted the initial linear region of the force–displacement data in the corresponding direction. More specifically, starting at 0.1 mm displacement, the equation of a line was repeatedly fit to force–displacement data over a gradually increasing displacement interval using MATLAB. The linear fit procedure was repeated until the R^2 value of the fit dropped below 0.995. The stiffness was then defined as the slope of the line that fit the data over the previous interval with $R^2 \geq 0.995$.

The width of the bonds was measured in both the CD and MD in ImageJ from the previously scanned images. The widths were measured by drawing segment lines in the center of the bond that were perpendicular to MD and CD, as illustrated in Figure 5. The stiffness and maximum force in the MD or CD were then scaled by a factor that was defined as the product of the

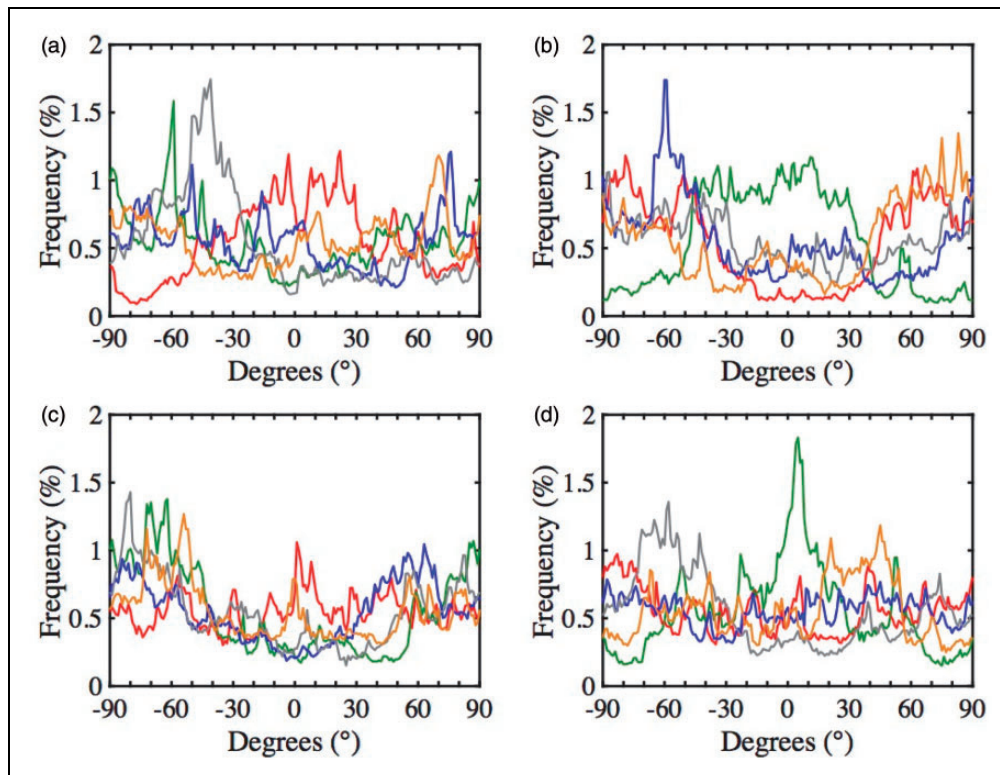


Figure 8. Orientation frequency histograms for (a) specimens 1–5, (b) specimens 6–10, (c) specimens 11–15, and (d) specimens 16–20. The corresponding force–displacement curves for these specimens are presented in Figure 6 using the same colors. The machine direction aligns with 0° and the cross-direction with 90° . (Color online only.)

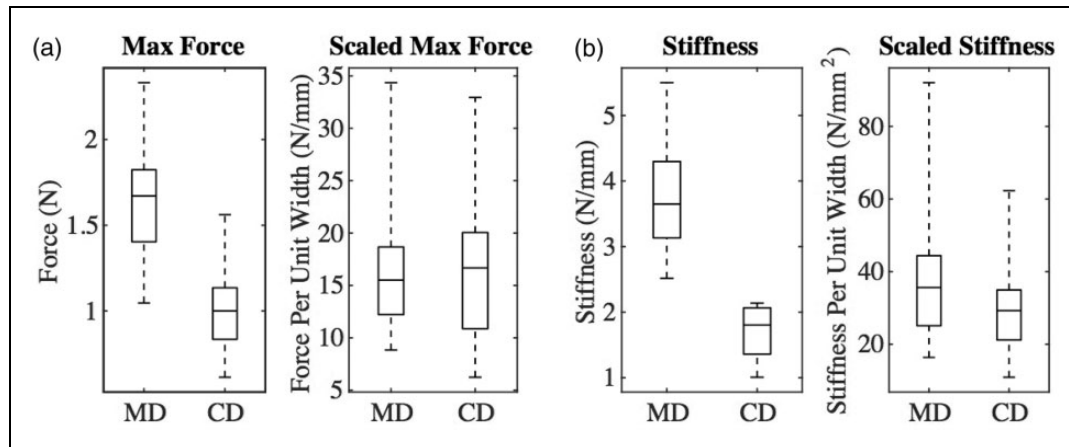


Figure 9. Box plots comparing the (a) maximum force and scaled maximum force and (b) stiffness and scaled stiffness in the machine direction (MD) and cross-direction (CD). The boxes represent the 25th and 75th percentiles. Scaling is done using the relative basis weight, orientation parameter, and bond width.

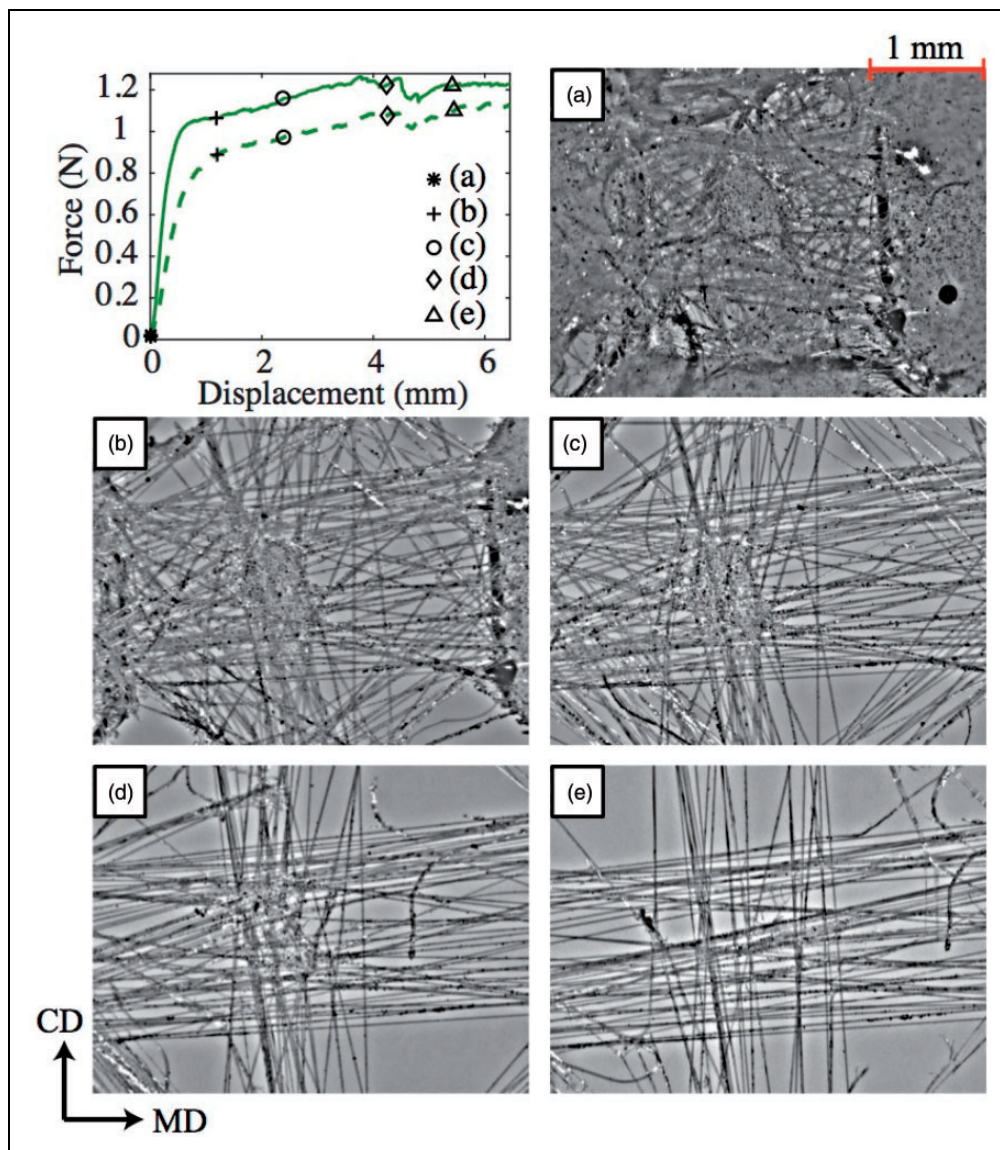


Figure 10. Force–displacement data correspond to the force–displacement curves reported in green in Figure 6(d). Disintegration of a bond at loads in the machine direction (MD) and cross-direction (CD) equal to (a) 0.021 and 0.015 N, (b) 1.06 and 0.890 N, (c) 1.16 and 0.972 N, (d) 1.22 and 1.07 N, and (e) 1.22 and 1.10 N, respectively.

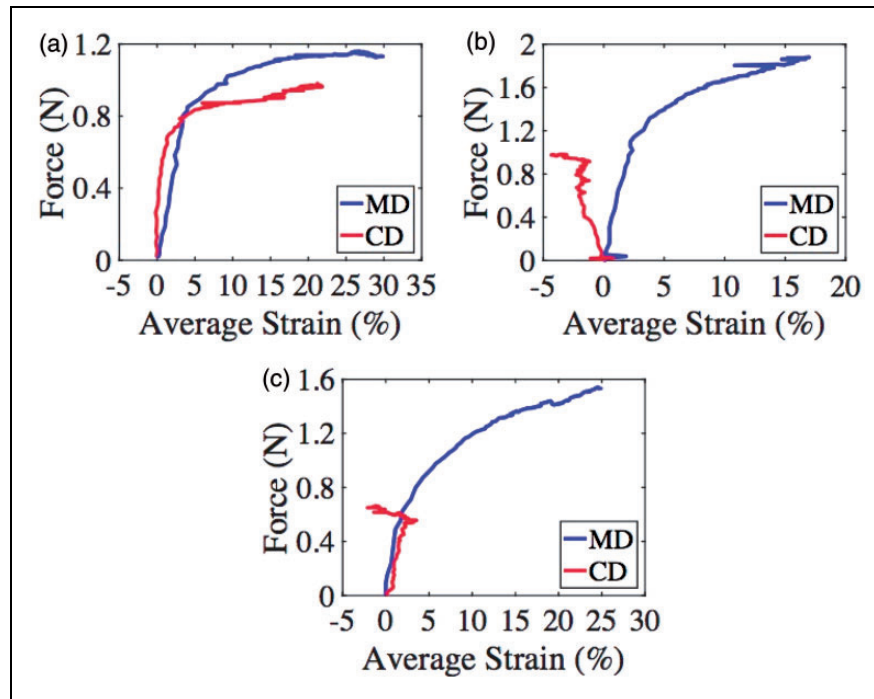


Figure 11. Force–strain curves obtained from three specimens subjected to equi-biaxial tests up to 2.3 mm displacements in the machine direction (MD) and cross-direction (CD). While the bonds always experienced positive strain in the MD, the bond experienced (a) consistently increasing strain, (b) consistently decreasing strain, and (c) a fluctuation between increasing and decreasing strain in the CD.

relative basis weight (B_{rel}) and the orientation parameter (O_p) and width of the bond (w) in the MD or CD, respectively.

Statistical analysis

Means and standard deviations were calculated for the maximum force, displacement at maximum force, stiffness, scaled maximum force, and scaled stiffness ($n=20$) in the MD and CD. The Student's t -test was used to compare the differences between these quantities in the MD and CD. The threshold for statistical significance was chosen to be 0.05. Statistical analysis was performed in MATLAB.

Results

The biaxial force–displacement data collected for each of the 20 specimens are presented in Figure 6. The force–displacement curves were linear at low displacements (<1 mm) and then became nonlinear in both the MD and CD. Every specimen reached a higher peak force in the MD than in the CD. Following these peak forces, small drops in the force–displacement curves were mainly observed. These likely resulted from the breakage of fibers forming the bond. The data were

then averaged at each displacement value in order to calculate an average force–displacement curve in the MD and CD. Figure 7 presents the average MD and CD force–displacement curves, in addition to force–displacement curves from all the specimens. This figure better represents the variation that was recorded among the force–displacement data.

The average maximum force in the MD was found to be 1.597 ± 0.316 N, and occurred at a displacement of 6.419 ± 1.840 mm. The average maximum force in the CD was 0.978 ± 0.255 N, and occurred at a displacement of 6.13 ± 1.296 mm. The maximum force was significantly higher in the MD than it was in the CD ($p = 1.10 \times 10^{-7} < 0.05$), but displacements at which the maximum force occurred were not statistically different in the MD and CD ($p = 0.554 > 0.05$). The average stiffness of the initial linear region of the force–displacement curve in the MD was 3.570 ± 0.806 N/mm, while in the CD the stiffness averaged 1.645 ± 0.410 N/mm. The difference in stiffness values in the MD and CD was statistically significant ($p = 2.05 \times 10^{-9} < 0.05$).

The fiber orientation frequency of each of the $2 \text{ mm} \times 2 \text{ mm}$ specimen, containing both the bond and surrounding fibers, is reported in Figure 8. The fiber orientation frequency (within 1° bins) is reported

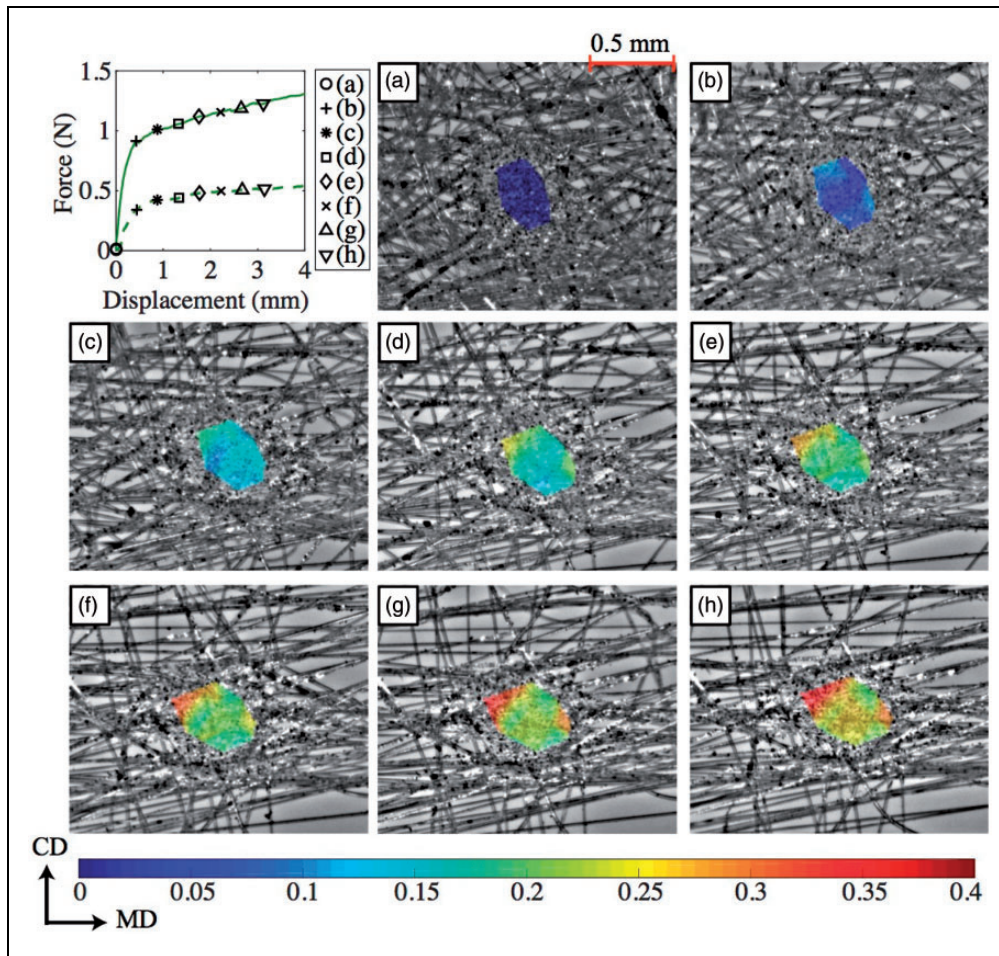


Figure 12. Force–displacement curves reported in green in Figure 6(b) for one specimen. Axial strain maps in the machine direction (MD) (e_{xx}) for a specimen at loads in the MD and cross-direction (CD) of (a) 0.012 and 0.011 N, (b) 0.914 and 0.241 N, (c) 1.02 and 0.426 N, (d) 1.06 and 0.440 N, (e) 1.12 and 0.481 N, (f) 1.16 and 0.496 N, (g) 1.18 and 0.501 N, and (h) 1.23 and 0.517 N, respectively.

relative to the MD. This figure indicates that overall the fibers were randomly oriented within each specimen, although in some specimens a preferred fiber orientation was noted. For example, in Figure 8(b), the orientation frequency curve in red indicates fewer fibers oriented in the MD compared to the fibers oriented closer to the CD. The corresponding force–displacement curves reported in red in Figure 6(b) show that the responses in the CD and MD were similar. On the other hand, the orientation frequency curve in green in Figure 8(b) indicates that there were more fibers oriented in the MD than in the CD. The corresponding force–displacement curves reported in green in Figure 6(b) show a clear difference in the specimen's mechanical behavior between the MD and CD, with the specimen reaching higher forces in the MD than in the CD.

The widths of the bond ranged from 0.480 to 0.660 mm in the CD and they ranged from 0.693 to

0.833 mm in the MD. As previously mentioned, the calculated stiffness and maximum forces were scaled by a scalar defined as the product of the relative basis weight, B_{rel} in equation (1), the orientation parameter, O_p in equation (2), and width of the bond, w_{CD} or w_{MD} in Figure 5. Both the orientation parameter and the relative basis weight are dimensionless, while the width of the bond has a dimension. Therefore, the scaled maximum force and stiffness have dimensions of N/mm and N/mm², respectively. The scaled maximum forces (per unit width) in the MD and CD were 16.5 ± 6.36 and 16.9 ± 7.07 N/mm, respectively. The scaled stiffness values (per unit width) in the MD and CD were 38.3 ± 18.0 and 29.0 ± 12.1 N/mm², respectively. The differences in the scaled maximum force (per unit width) and stiffness (per unit width) in the MD and CD were not statistically significant ($p=0.884 > 0.05$ and $p=0.144 > 0.05$, respectively). Box plots comparing the maximum force, stiffness,

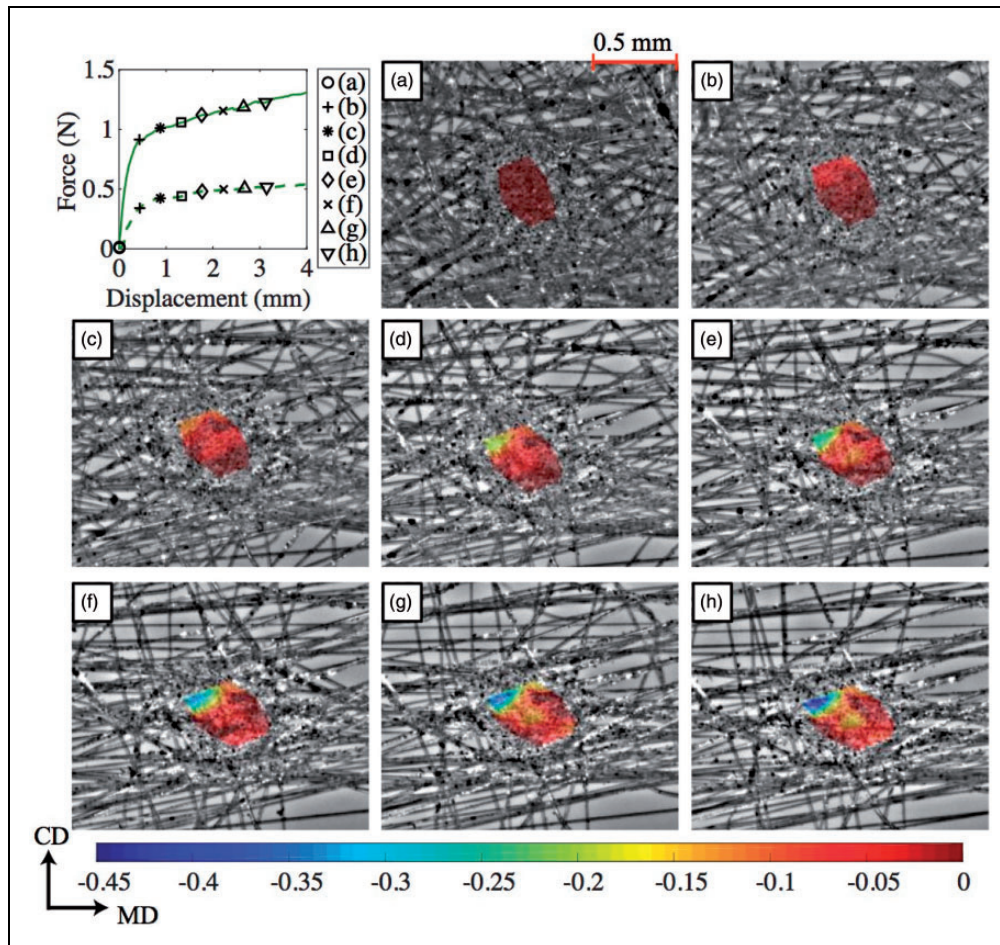


Figure 13. Force–displacement curves reported in green in Figure 6(b) for one specimen. Axial strain maps in the cross-direction (CD) (ϵ_{yy}) for the same specimen in Figure 12, also at loads in the machine direction (MD) and CD of (a) 0.012 and 0.011 N, (b) 0.914 and 0.241 N, (c) 1.02 and 0.426 N, (d) 1.06 and 0.440 N, (e) 1.12 and 0.481 N, (f) 1.16 and 0.496 N, (g) 1.18 and 0.501 N, and (h) 1.23 and 0.517 N, respectively.

scaled maximum force, and scaled stiffness are presented in Figure 9. Thus, by taking into account the relative basis weight, orientation of the fibers, and width of the bond, the difference between the stiffness and maximum force in the MD and the CD was reduced (Figure 9). Similarly, in previous studies by Jubera et al.,¹⁸ the nonwoven uniaxial tensile properties were also found to be similar in the MD and CD when measuring force per unit width. Future work should verify that the scaling proposed here can be extended to bonds in nonwovens having a variety of relative basis weights, since in this study bonds with comparable relative basis weights were selected.

The behavior of the bond was visualized through the images collected during biaxial testing. In all of the tests, the bond was observed to gradually disintegrate into fibers, as shown in Figure 10. The fibers used for the nonwoven were bi-component, composed of a PE sheath and PP core, and were thermomechanically

bonded at discrete points. The temperature at which these bonds were formed was likely high enough to melt the PE of the sheath, but not the PP of the core. Therefore, when the bonds were pulled in tension, the fused PE film likely broke, but the PP core of the fibers remained intact. These fibers then became the load bearing components of the specimen and often re-oriented until their failure occurred.

The average strain was computed for all specimens up to 2.3 mm displacement. The forces at this displacement were $86.4\% \pm 4.4\%$ of the maximum force in the MD and $84.3\% \pm 7.2\%$ of the maximum force in the CD. The application of the DIC method for non-contact strain measurement to nonwovens had limitations. For the tested specimens, the tracking points had to be manually selected due to the inability to achieve sufficiently dense speckle patterns. Moreover, individual tracking points often disappeared or dislodged from the bond, especially when fibers were pulled out of

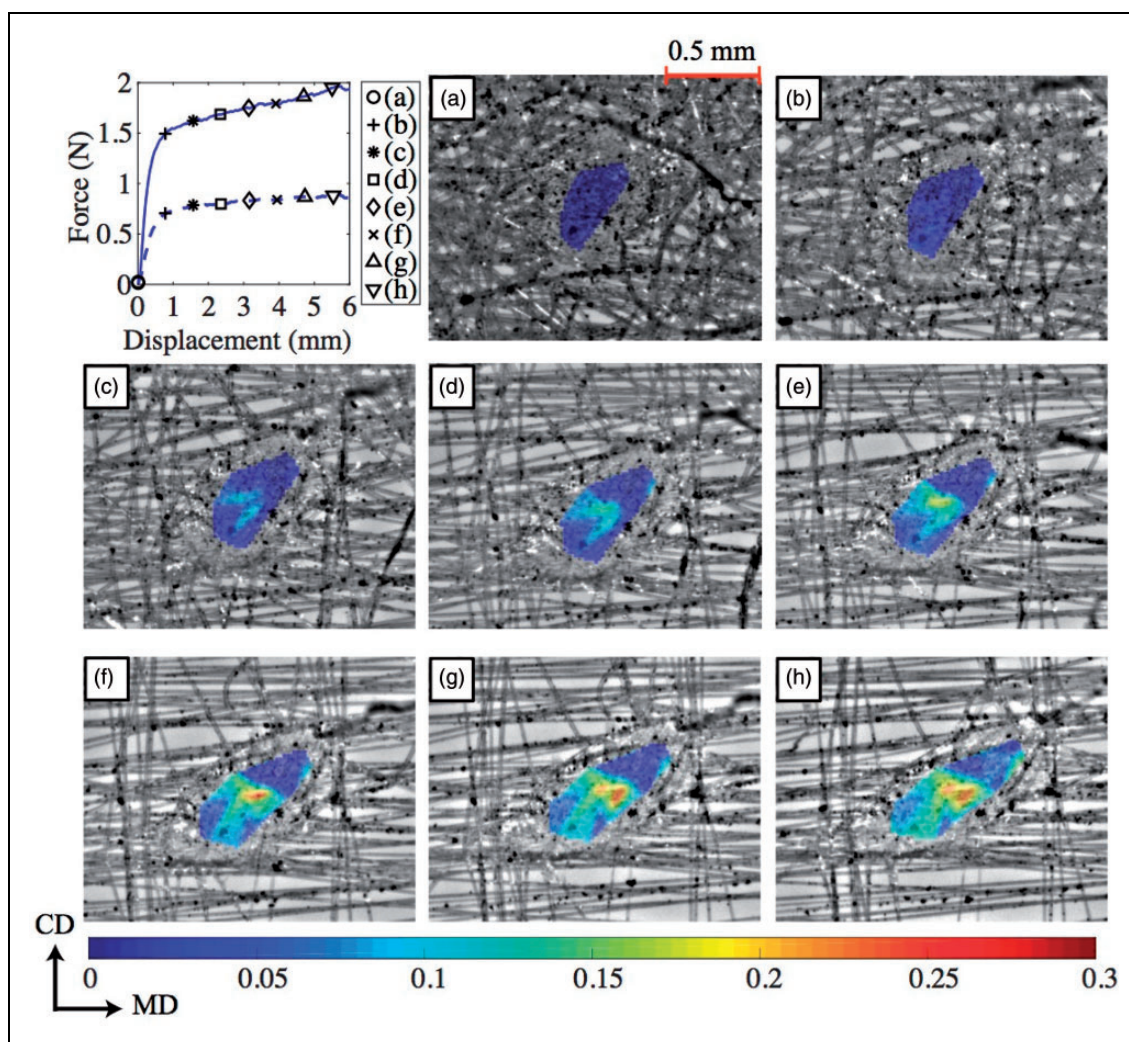


Figure 14. Force–displacement curves reported in blue in Figure 6(b) for one specimen. Shear strain maps in the machine direction (MD)/cross-direction (CD) plane (e_{xy}) for a specimen at loads in the MD and CD of (a) 0.015 and 0.014 N, (b) 1.49 and 0.702 N, (c) 1.62 and 0.788 N, (d) 1.69 and 0.799 N, (e) 1.75 and 0.831 N, (f) 1.79 and 0.837 N, (g) 1.86 and 0.869 N, and (h) 1.95 and 0.882 N, respectively.

the bond. The fibers also occasionally moved over the plane containing the bond, obstructing the field of view, and preventing points on the bond from being tracked. Thus, the average strain was analyzed up to 2.3 mm because, after this displacement, too much damage or movement of the speckles within the bond occurred and the speckles could not be readily tracked. The complex structure of the bonds of the nonwoven fabric made the analysis process time consuming.

While the specimens were equally displaced in both the MD and CD, the average normal strain experienced by the individual bonds was not equal in these directions. The average shear strain was measured but was negligible for most, but not all, specimens. The average strain in the MD and average strain in the CD were plotted against the corresponding forces for some

specimens (Figure 11). For all the specimens, the average strain in the MD increased with load, while the average strain in the CD varied among consistently increasing (Figure 11(a)), consistently decreasing (Figure 11(b)), and increasing and decreasing irregularly (Figure 11(c)). Mostly, the average strain was often negative in the CD. This was very likely caused by the presence of fewer fibers in the CD. The fibers being pulled in the MD caused the bond to collapse in the CD and, for this reason, the bond experienced negative strain in the CD. Fluctuations in the strain were likely due to fibers straightening out and becoming load bearing and/or fiber breakage. Kim et al.²⁶ previously reported variation in the strain response of individual bonds. These authors tested nonwoven specimens with multiple bonds but strain measurements were

performed on individual bonds, and the strain varied from increasing to decreasing. Future biaxial tests should be performed at higher displacement rates in the CD than in the MD, rather than at equal displacement rates in the two directions, in order to generate positive strain in the CD.

Strain maps were generated for selected specimens to compute the local (rather than average) strain in the MD and CD within the bond. Representative maps are reported in Figures 12 and 13. In the MD, the overall bond strained but as the specimen approached displacements in the MD and CD of 3 mm, a region of high strain developed within the bond (top-left region, Figure 12(h)). The same specimen in the CD experienced minimal strain, but similar to the MD, an area of high compressive strain developed in one region (top region, Figure 13(h)). For one specimen, the bond was observed to undergo shear (Figure 14). By developing the strain map, the shear strain was found to be significant but was highly localized, occurring within a small portion of the bond (Figure 14(h)). Overall, Figures 12–14 show that the strain within the bond was highly inhomogeneous. It must be noted that fiber straightening caused speckles near the border of the bond to disappear and, thus, these points could not be tracked. Due to these limitations, the strain map could only be obtained in the central region of the bond and not at its border (Figures 12–14).

Conclusions

In this study, new experimental methods for examining the biaxial response of individual bonds in a thermo-mechanically bonded nonwoven fabric are presented. The maximum force and stiffness in the MD were statistically higher than in the CD. After scaling the maximum force and stiffness by a scalar defined as the product of the relative basis weight, fiber orientation parameter, and width of the bond, these quantities in the two directions were found to be statistically equivalent. This indicates that the biaxial response of the bond was strongly dependent on the relative basis weight, orientation parameter, and width. The bonds in the specimens were consistently observed to disintegrate and return to their original constituent fibers. Strains in the MD were consistently positive and increasing, while strains in the CD varied from increasing to decreasing. This variation was likely dependent on the number of fibers in each direction. Strain maps displayed the inhomogeneity of bonds. New knowledge about the biaxial tensile properties of individual bonds in nonwovens will enable manufacturers to make informed decisions about producing or selecting nonwoven materials and their ultimate applications. While this experimental study focuses on bonds with

specific geometry, orientation of fibers, and relative basis weight in one type of commercial nonwoven fabric, the new testing techniques developed can be extended to other nonwoven fabrics, including those made with a range of processing variables, such as bonding temperature and fiber composition.

Declaration of conflicting interests

The authors declared no potential conflicts of interest with respect to the research, authorship, and/or publication of this article.

Funding

The authors received no financial support for the research, authorship, and/or publication of this article.

References

1. Russell SJ. *Handbook of nonwovens*. Cambridge, England: Woodhead Publishing, 2006.
2. Albrecht W, Fuchs H and Kittelmann W. *Nonwoven fabrics: raw materials, manufacture, applications, characteristics, testing processes*. Weinheim, Germany: John Wiley & Sons, 2006.
3. Suslick KS. *Kirk-Othmer encyclopedia of chemical technology*. Vol. 26, New York: John Wiley & Sons, 1998, pp.517–541.
4. Srinivasan J and Kathirvelu S. An introduction to spunbond and meltblown nonwovens. *Synth Fibres* 2006; 35: 27.
5. Dasdemir M, Maze B, Anantharamaiah N, et al. Influence of polymer type, composition, and interface on the structural and mechanical properties of core/sheath type bicomponent nonwoven fibers. *J Mater Sci* 2012; 47: 5955–5969.
6. Dharmadhikary RK, Gilmore TF, Davis HA, et al. Thermal bonding of nonwoven fabrics. *Text Prog* 1995; 26: 1–37.
7. Kim HS. Relationship between fiber orientation distribution function and mechanical anisotropy of thermally point-bonded nonwovens. *Fibers Polym* 2004; 5: 177–181.
8. Demirci E, Acar M, Pourdeyhimi B, et al. Finite element modelling of thermally bonded bicomponent fibre nonwovens: tensile behaviour. *Comput Mater Sci* 2011; 50: 1286–1291.
9. Sozumert E, Farukh F, Demirci E, et al. Damage mechanisms of random fibrous networks. *J Phys Conf Ser* 2015; 628: 012093.
10. Farukh F, Demirci E, Sabuncuoglu B, et al. Mechanical analysis of bi-component-fibre nonwovens: finite-element strategy. *Composites Part B* 2015; 68: 327–335.
11. Gao X and Wang L. Finite element modelling for tensile behaviour of thermally bonded nonwoven fabric. *Autex Res J* 2015; 15: 48–53.
12. Wang H, Jin X, Mao N, et al. Differences in the tensile properties and failure mechanism of PP/PE core/sheath bicomponent and PP spunbond fabrics in uniaxial conditions. *Text Res J* 2010; 80: 1759–1767.

13. Nanjundappa R and Bhat GS. Effect of processing conditions on the structure and properties of polypropylene spunbond fabrics. *J Appl Polym Sci* 2005; 98: 2355–2364.
14. Kim HS, Pourdeyhimi B, Desai P, et al. Anisotropy in the mechanical properties of thermally spot-bonded nonwovens: experimental observations. *Text Res J* 2001; 71: 965–976.
15. Bhat GS, Jangala PK and Spruiell JE. Thermal bonding of polypropylene nonwovens: effect of bonding variables on the structure and properties of the fabrics. *J Appl Polym Sci* 2004; 92: 3593–3600.
16. Goswami BC, Suryadevara J and Vigo TL. Determination of Poisson's ratio in thermally bonded nonwoven fabrics. *Text Res J* 1984; 54: 391–396.
17. Ridruejo A, González C and Llorca J. Failure locus of polypropylene nonwoven fabrics under in-plane biaxial deformation. *Comptes Rendus Mécanique* 2012; 340: 307–319.
18. Jubera R, Ridruejo A, González C, et al. Mechanical behavior and deformation micromechanisms of polypropylene nonwoven fabrics as a function of temperature and strain rate. *Mech Mater* 2014; 74: 14–25.
19. Ridruejo A, Jubera R, González C, et al. Inverse notch sensitivity: cracks can make nonwoven fabrics stronger. *J Mech Phys Solids* 2015; 77: 61–69.
20. Sutton MA, Orteu JJ and Schreier H. *Image correlation for shape, motion and deformation measurements: basic concepts, theory and applications*. Springer Science & Business Media, 2009.
21. Chhabra R, Gruenbacher DP, Monebrake DW, et al. Composite filter substrate comprising a mixture of fibers. Patent application 14/576,252, USA, Google Patents, 2014.
22. Eberl C, Thompson R, Gianola D, et al. Digital image correlation and tracking. MatLabCentral, Mathworks file exchange server, FileID. 2006, 12413.
23. Sage D. OrientationJ: ImageJ's plugin for directional analysis in images, 2012.
24. Püspöki Z, Storath M, Sage D, et al. Transforms and operators for directional bioimage analysis: a survey. In: *Focus on bio-image informatics*. Springer, 2016, pp.69–93.
25. Cox HL. The elasticity and strength of paper and other fibrous materials. *Br J Appl Phys* 1952; 3: 72.
26. Kim HS, Deshpande A, Pourdeyhimi B, et al. Characterizing structural changes in point-bonded nonwoven fabrics during load-deformation experiments. *Text Res J* 2001; 71: 157–164.